© 2018. Published by The Company of Biologists Ltd | Development (2018) 145, dev156604. doi:10.1242/dev.156604

RESEARCH ARTICLE

Slow calcium waves mediate furrow microtubule reorganization and germ plasm compaction in the early zebrafish embryo

Celeste Eno[1], Timothy Gomez[2], Diane C. Slusarski[3] and Francisco Pelegri[1,*]

ABSTRACT

Zebrafish germ plasm ribonucleoparticles (RNPs) become recruited to furrows of early zebrafish embryos through their association with astral microtubules ends. During the initiation of cytokinesis, microtubules are remodeled into a furrow microtubule array (FMA), which is thought to be analogous to the mammalian midbody involved in membrane abscission. During furrow maturation, RNPs and FMA tubules transition from their original distribution along the furrow to enrichments at the furrow distal ends, which facilitates germ plasm mass compaction. We show that *nebel* mutants exhibit reduced furrow-associated slow calcium waves (SCWs), caused at least in part by defective enrichment of calcium stores. RNP and FMA distal enrichment mirrors the medial-to-distal polarity of SCWs, and inhibition of calcium release or downstream mediators such as Calmodulin affects RNP and FMA distal enrichment. Blastomeres with reduced or lacking SCWs, such as early blastomeres in *nebel* mutants and wild-type blastomeres at later stages, exhibit medially bundling microtubules similar to midbodies in other cell types. Our data indicate that SCWs provide medial-to-distal directionality along the furrow to facilitate germ plasm RNP enrichment at the furrow ends.

KEY WORDS: Calcium, Germ plasm, Ribonucleoparticles, Microtubules, F-actin, Zebrafish

INTRODUCTION

In the zebrafish *Danio rerio*, as in many animal species, primordial germ cell specification is mediated by the maternal inheritance of the germ plasm, a specialized cytoplasm containing specific RNAs and proteins (Wylie, 1999; Strome and Lehmann, 2007; Eno and Pelegri, 2013). Zebrafish germ plasm ribonucleoparticles (RNPs) are inherited as spherical units, typically of less than 1 µm in diameter, that are initially dispersed through the blastodisc. During the first several embryonic divisions, these units multimerize, gathering into clusters while appearing to retain their initial spherical structure (Theusch et al., 2006; Eno and Pelegri, 2013; Nair et al., 2013; Eno and Pelegri, 2018).

During the early embryonic cell divisions, RNP aggregates move to the forming furrows to generate typically four germ plasm masses (Yoon et al., 1997; Pelegri et al., 1999; Knaut et al., 2000). These aggregates subsequently become incorporated into primordial germ cells (Olsen et al., 1997; Yoon et al., 1997; Braat et al., 1999; Knaut et al., 2000), where they are necessary and sufficient for germ cell specification (Hashimoto et al., 2004; Bontems et al., 2009; Miranda-Rodríguez et al., 2017).

The assembly of germ plasm masses at the furrows involves sequential steps. First, RNP multimers assemble even prior to furrow initiation (pre-aggregation). Second, RNP pre-aggregates gather locally towards the forming furrows (furrow recruitment). Both of these processes appear to be mediated by the outward growth of astral microtubules, the tips of which are associated with germ plasm RNPs (Theusch et al., 2006; Eno and Pelegri, 2013; Nair et al., 2013). Germ plasm recruitment during furrow formation results in the accumulation of RNP aggregates collectively forming an elongated, rod-like structure along most of the length of the furrow. At the same time, microtubules form the furrow microtubule array (FMA) (Danilchik et al., 1998; Jesuthasan, 1998), which is thought to be homologous to the mammalian midbody involved in cell abscission (Otegui et al., 2005). FMA tubules are initially arranged in parallel along the length of the furrow, oriented perpendicular to the cleavage plane, with germ plasm RNP aggregates recruited along the furrow maintaining their association with microtubule ends. A third step in the germ plasm segregation process, 'distal compaction', occurs during furrow maturation and involves coordinated changes in both RNP aggregates at the furrow and the FMA (Fig. 1). During this step, RNPs recruited at the furrow translocate towards the nearest furrow distal end, where they form compact RNP masses (Pelegri et al., 1999). At the same time, FMA tubules become enriched and undergo bundling in the distal furrow region, while their ends, which maintain their association with germ plasm RNPs, acquire a characteristic outward tilt. As the furrow is completed, FMA microtubules become disassembled leaving the compacted germ plasm mass at the furrow distal end (Pelegri et al., 1999).

Germ plasm pre-aggregation, furrow recruitment and distal compaction therefore achieve the purpose of gathering maternally inherited single RNPs into discrete structures that will be subsequently inherited by primordial germ cells. In the accompanying article (Eno and Pelegri, 2018), we show that mutations in the maternal effect gene *mid1ip1l* (also known as *aura*), which encodes the cytoskeletal regulator Mid1ip1l, result in defects in the recruitment of germ plasm RNPs to the furrows. This function is mediated through *mid1ip1l*-dependent cortical F-actin dynamics and contractions associated with germ plasm RNPs, which allow RNP retention at the cortex prior to furrow formation and likely also facilitate RNP multimerization during furrow maturation. Here, we focus on the process of distal compaction and document a calcium-dependent mechanism required for the enrichment of germ plasm RNPs, together with associated FMA, to the distal ends of the furrow.

In both zebrafish and medaka, waves of intracellular calcium increase are associated with zebrafish cytokinesis during the first

[1]Laboratory of Genetics, University of Wisconsin – Madison, Madison, WI 53706, USA. [2]Department of Neuroscience, University of Wisconsin – Madison, Madison, WI 53705, USA. [3]Department of Biology, The University of Iowa, Iowa City, IA 52242, USA.

*Author for correspondence (fjpelegri@wisc.edu)

T.G., 0000-0002-1515-8228; D.C.S., 0000-0003-3793-8636; F.P., 0000-0002-0464-7042

Received 20 July 2017; Accepted 27 March 2018

Development (2018) 145, dev156604. doi:10.1242/dev.156604

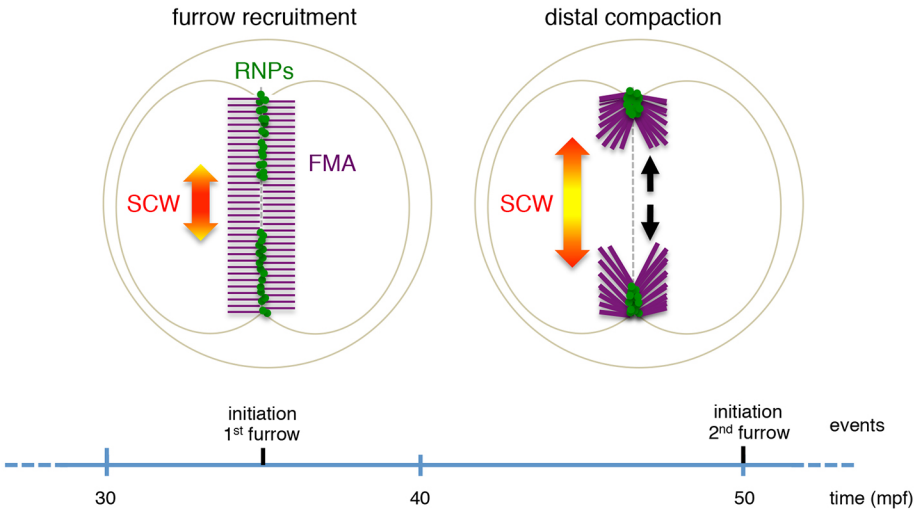

Fig. 1. Germ plasm and FMA reorganization. During furrow formation, germ plasm ribonucleoparticles (RNPs) and associated furrow microtubule array (FMA) become enriched to the furrow distal ends. Waves of intracellular calcium [slow calcium waves (SCWs)] travel in a medial-to-distal orientation, with the maturation wave occurring during furrow formation (shown offset from the furrow plane for clarity).

several cell cleavage cycles (Fluck et al., 1991; Chang and Meng, 1995; Reinhard et al., 1995; Webb et al., 1997; Créton et al., 1998). These waves have been termed slow calcium waves (SCWs) (Fig. 1) owing to their relatively low speed of propagation (0.1-1 µm/s) (Jaffe, 1993). Two primary furrow-associated SCWs have been described. A superficial 'initiation wave', generated just prior to the appearance of the furrow cleft, is required for furrow formation. Subsequently, a larger 'maturation wave' penetrates deeper into the cytoplasm and has a role in events associated with furrow maturation, such as vesicle exocytosis and the formation of F-actin-dependent lamellipodia (Lee et al., 2003; Li et al., 2008).

The intracellular calcium signaling network is complex and the release of calcium from internal stores is controlled by three primary sets of ligands and calcium channels: inositol trisphosphate (IP_3) and cyclic adenosine diphosphate ribose (cADPR) through IP_3 and ryanodine receptors, respectively, both at the endoplasmic reticulum (ER), and nicotinic acid adenine dinucleotide phosphate (NAADP) through NAADP-sensitive channels on lysosome-like organelles (Berridge et al., 2003). Previous studies have shown the presence of calcium stores activated by IP_3 and NAADP, but not cADPR, in early zebrafish embryos, and that inhibition of IP_3 receptors affects furrow formation in early blastomeres (Lee et al., 2003).

Embryos from homozygous *nebel* mutant females exhibit normal nuclear division and furrow initiation, but the forming furrows either fail to develop a fully adhesive membrane septum between daughter cells or undergo regression, revealing a defect in the completion of cytokinesis (Pelegri et al., 1999). In *nebel* mutant embryos, germ plasm RNP aggregates form compact masses and FMA tubule tips undergo bundling, but these events occur in medial, rather than distal, regions of the furrow.

Several factors are known to mediate RNP aggregate and FMA dynamics in early embryonic blastomeres. In myosin-inhibited embryos, the RNP aggregate and FMA are arrested in a conformation corresponding to furrow initiation, namely as an elongated RNP aggregate along the furrow with the FMA retaining its original parallel conformation (Urven et al., 2006). A similar reorganization defect occurs in *mid1ip1l* mutant embryos, likely because of the function of this gene in F-actin reorganization (Eno et al., 2016; Eno and Pelegri, 2018). Recent studies have shown that inhibition of the small GTPase RhoA and its effector ROCK result in aberrant enrichment of germ plasm in medial regions of the mature furrow, a defect similar to that observed in *nebel* mutants (Miranda-Rodríguez et al., 2017). However, mechanisms underlying germ plasm and FMA reorganization, including cues conferring medial-to-distal directionality along the furrow plane, remain largely unknown.

Here, we show that during the early cleavage stages, *nebel* mutant embryos show reduced intensity and temporal dynamics of furrow-associated SCWs. Treatments that interfere with SCW formation also result in defects in germ plasm RNP and FMA distal enrichment. Under these conditions, FMA bundles inward, as in later blastomeres that lack SCWs. Germ plasm RNP aggregate compaction and FMA bundling direction correlate with the medial-to-distal directionality of SCWs and are dependent on Calmodulin activity. Our studies indicate that SCWs in the early embryo modify RNP distribution and microtubule reorganization during furrow maturation, in order to facilitate the formation of multiple germ plasm masses capable of inducing the germ cell fate.

RESULTS

nebel mutant embryos show defects in furrow-associated SCWs

Because of the proposed role for SCWs in early teleost embryo furrow formation (Chang and Meng, 1995; Webb et al., 1997; Créton et al., 1998; Li et al., 2008), we visualized SCWs in wild-type and *nebel* mutant embryos with intracellular calcium-sensitive dyes. We first used the ratiometric indicator Fura-2-Dextran, which allows for quantitation of intracellular calcium levels. The patterns of intracellular calcium concentration in wild type and *nebel* mutants were markedly different. As previously reported (Chang and Meng, 1995; Webb et al., 1997; Créton et al., 1998; Li et al., 2008), intracellular calcium increases appear in wild-type embryos immediately prior to furrow initiation and during furrow maturation, corresponding to initiation and maturation SCWs, with the maturation SCW showing calcium release of greater intensity and depth (Fig. 2A, Fig. S1A, Movie 1). By contrast, *nebel* mutants exhibit intracellular SCWs of reduced amplitude and frequency (see below) compared with wild type (Fig. 2B, Fig. S1B, Movie 2). Embryos mutants for *mid1ip1l*, another maternal effect mutation affecting late cytokinesis (Pelegri et al., 2004; Eno et al., 2016), exhibit normal furrow-associated SCWs (data not shown), indicating that the SCW defect in *nebel* is not a general consequence of failed completion of cytokinesis.

To better study the relationship between SCWs and furrow development, we scored wild-type and mutant embryos for defects during furrow initiation and completion (Table S2). Nearly all

Development (2018) 145, dev156604. doi:10.1242/dev.156604

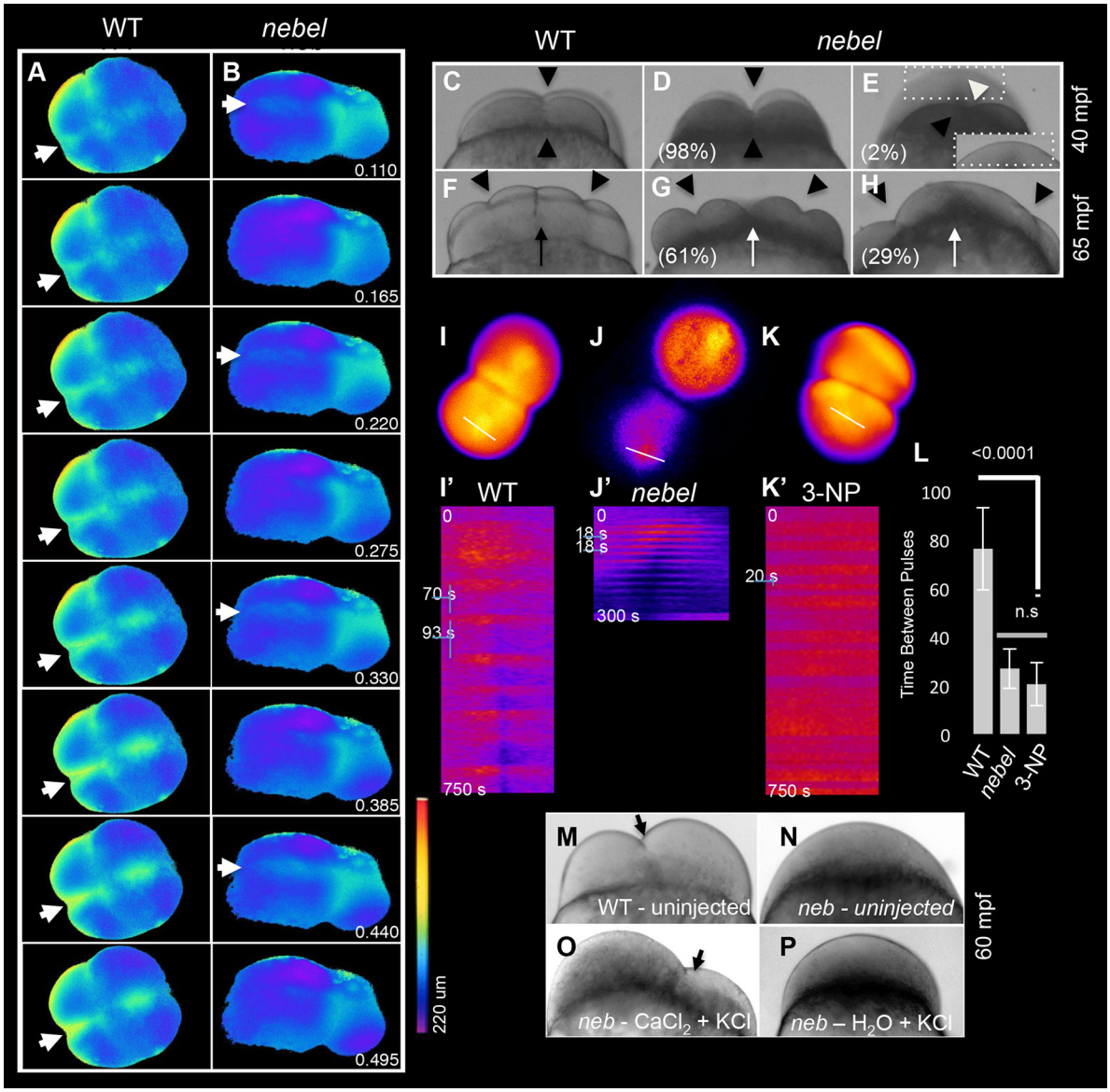

Fig. 2. Reduced calcium release underlies furrow formation defects in zebrafish *nebel* mutants. (A,B) Fluorescence after injection of Fura-2 during second cleavage furrow formation, with calcium-saturated (340 nm) and calcium-free (380 nm) images converted to a pseudocolor ratio. Intracellular calcium increases are observed prior to and during furrow formation in wild-type embryos (A), whereas *nebel* mutants show repeated intracellular increases of reduced intensity (B). Animal views, with numbers indicating the lapsed fraction of the cell cycle. Arrows indicate sites of high intracellular calcium, corresponding to SCWs. (C-H) In *nebel* mutants, furrow initiation appears normal [black arrowheads during the first (D,E versus C) and third (G,H versus F) cell division]. In rare cases, the furrow fails to initiate (white arrowhead in E; insert depicts a clearer focal plane). Black arrow (F) indicates the adhesive septum in wild type, which fails to form in mutants (G,H, white arrows). (I-L) Ratiometric analysis using Oregon Green 488 BAPTA-Dextran and Rhodamine in wild-type (I), *nebel* mutant (J) and 3-NP-treated wild-type (K) embryos, with representative kymographs (I′-K′, white line in I-K) and average time in seconds between calcium pulses (L, n>6 furrows). Error bars indicate the s.e.m.; two-tailed P-values were assessed using an unpaired t-test. (M-P) Pseudocleavages in unfertilized wild-type eggs (M, arrow) do not form in *nebel* mutant eggs (N) but are induced by $CaCl_2$ injection (O), an effect independent of the KCl co-injected to improve egg survival (P).

cleaving *nebel* mutant embryos (98%, n=255) underwent normal furrow initiation (Fig. 2D) at a time and extent similar to wild type (Fig. 2C). However, these mutant embryos invariably showed defects in furrow completion, such as a lack of formation of a cell adhesive wall or furrow regression (Fig. 2G,H, compared with 2F). Only in rare cases (2%) did blastomeres exhibit defects in furrow initiation, as reflected by lack of furrowing in one of two blastomeres in the 2-cell stage embryo (Fig. 2E). These observations confirm our previous conclusions that *nebel* largely affects late stages of cytokinesis (Pelegri et al., 1999), and further suggest that *nebel* function is required to achieve high calcium release levels characteristic of the maturation SCW. As opposed to the two primary SCWs found in wild type, with the maturation SCW lasting most of furrow formation, the SCWs of reduced intensity observed in *nebel* mutants appeared to fluctuate, with up to four waves of calcium release observed in a single cycle and a relatively constant periodicity of ~7 min (Fig. 2B).

The defects in intracellular calcium release were also observed using the calcium-sensitive dye Oregon Green 488 BAPTA-Dextran, which does not allow measurement of absolute intracellular calcium concentration but does allow improved visualization and quantification of SCWs. Imaging of wild-type embryos with this dye readily reveals SCWs at the furrow (Fig. 2I), with kymograph analysis showing an average time between peaks of

Development (2018) 145, dev156604. doi:10.1242/dev.156604

76 s (s.d.=16.9 s, *n*=38 peaks from 8 embryos; Fig. 2I′,L, Fig. S2). By contrast, *nebel* mutants exhibit a higher frequency of SCWs, with an average period between peaks of 27 s (s.d.=8.1 s, *n*=56 peaks from 8 embryos; Fig. 2J,J′,L, Fig. S2). As expected, exposure of embryos to the IP_3 receptor inhibitor 2-APB results in the rapid cessation of calcium release at the furrow (Lee et al., 2003) (data not shown). Thus, our data show that *nebel* mutant embryos exhibit defects in furrow-associated SCWs, such as a reduction in magnitude and increase in frequency of intracellular calcium release.

Intracellular calcium rescues aspects of the *nebel* mutant phenotype

If the *nebel* mutant phenotype is caused by reduced intracellular calcium release, the furrow defect may be rescued by an increase in intracellular calcium. Initial experiments involving $CaCl_2$ injections into cleaving embryos did not result in significant rescue of the *nebel* mutant cellularization defect (data not shown), possibly because of the need for precise spatiotemporal regulation of calcium release at the forming furrow. However, we took advantage of differences between unfertilized eggs from wild-type and *nebel* mutant females (Pelegri et al., 1999) to test whether calcium can rescue the *nebel* mutant phenotype (Table S3). After egg activation, unfertilized eggs from wild-type females typically exhibit asymmetric membrane ingression, also known as pseudocleavages (Fig. 2M) (Kane and Kimmel, 1993), possibly through the unregulated exocytosis of intracellular membrane (data not shown; see also Danilchik et al., 1998). In contrast to wild type, activated yet unfertilized eggs from *nebel* mutant females typically fail to form pseudocleavages (6%, *n*=125; Fig. 2N). Injection of 0.1 mM or 0.2 mM $CaCl_2$ into eggs from *nebel* mutant females significantly increased pseudocleavage formation [to 42% (*n*=111) or 54% (*n*=115), respectively; Fig. 2O], whereas control injection did not have this effect (6%, *n*=123; Fig. 2P). Thus, the absence of pseudocleavage formation in unfertilized *nebel* mutant eggs can be reversed by introducing calcium, consistent with a reduction in intracellular calcium as an underlying basis for the *nebel* mutant phenotype.

Mitochondrial function is required for SCW dynamics

Previous studies have demonstrated the ability of calcium buffering by mitochondria to influence the magnitude and patterns of intracellular calcium waves (Jouaville et al., 1995; Babcock et al., 1997). Specifically, mitochondrial activity is directly correlated to the amplitude and inversely correlated to the frequency of IP_3-induced propagating calcium waves in the *Xenopus* oocyte cortex (Jouaville et al., 1995). Because these effects are reminiscent of those found in furrow-associated SCWs in *nebel* mutants, we tested whether inhibition of mitochondrial activity leads to defects in SCWs in wild-type embryos. Indeed, wild-type embryos exposed during furrow formation to the mitochondrial respiratory Complex II inhibitor 3-nitropropionic acid (Alston et al., 1977) exhibited reduced intensity and increased frequency of SCWs (Fig. 2K,K′,L, Fig. S2). Thus, similar to propagating calcium waves in *Xenopus* oocytes, furrow-associated SCWs in early zebrafish embryos require functional mitochondrial activity.

Calcium stores are present in *nebel* mutants but fail to become enriched to the furrow

Previous studies have shown that IP_3- and NAADP-dependent, but not cADPR-dependent, calcium stores are present and active in the early zebrafish embryo (Lee et al., 2003). To test whether *nebel* mutants contain functional calcium stores, the calcium release response to injection of IP_3 or NAADP was compared with that of wild-type embryos (Fig. 3A). Agonist was injected into unfertilized embryos in order to reduce experimental variation caused by the uneven distribution of calcium stores at the vicinity of forming furrows (Berridge, 1993; Berridge et al., 2003; Lawrence and Mandato, 2013) (see also Fig. 4). As expected from previous studies (Lee et al., 2003), both IP_3 and NAADP injections (Fig. 3D,F), but not mock injections (Fig. 3B), elicit a calcium release response in wild type. These two agonists (Fig. 3E,G), but not control injections (Fig. 3C), elicited a calcium release response similar in magnitude to that in *nebel* mutants (Fig. 3H). Consistent with the proposed role of IP_3 in long-range calcium wave propagation through calcium-mediated calcium release (Finch et al., 1991; Galione et al., 1993), the spatial extent of calcium release after IP_3 injection expands into most of the blastodisc (Fig. 3D,E), whereas it is comparatively confined after NAADP injection (Fig. 3F,G), with wild type and *nebel* mutants exhibiting a similar behavior (Fig. 3I). Together, our data indicate that *nebel* mutant eggs are able to elicit an apparently normal calcium release response to IP_3 and NAADP, suggesting that the IP_3- and NAADP-sensitive calcium stores and the corresponding receptors are present and functional in mutant eggs and embryos.

Since *nebel* mutant embryos exhibit reduced SCWs, yet the eggs exhibit a robust response to calcium agonists, we tested whether the localization patterns of calcium stores are affected in mutant embryos. Labeling with $DiOC_6$ shows an enrichment of ER at the furrows of early wild-type embryos (Fig. 4A). By contrast, the ER fails to become enriched at the furrows in *nebel* mutants, being found instead in a diffuse pattern throughout the blastodisc (Fig. 4B). Using Lysotracker as a labeling dye, we find that lysosomes also become aggregated to the forming furrows in wild-type embryos (Fig. 4C). *nebel* mutant embryos, on the other hand, lack an enrichment of lysosomes at the furrow, which instead accumulate in peripheral regions of the embryo (Fig. 4D). Labeling with Mitotracker shows that mitochondria exhibit a similar pattern to that of ER, with enrichment at the furrows in wild type (Fig. 4E) but distributed in a diffuse pattern in *nebel* mutants (Fig. 4F). Thus, *nebel* mutants show a general defect in the enrichment of calcium stores at the forming furrow, including the ER, lysosomes and mitochondria. Given the essential role for these stores and their localization in regulated calcium release (Jouaville et al., 1995; Babcock et al., 1997; Lee et al., 2003), this defect is likely to be a primary cause for the observed effects on furrow-associated SCWs in these mutants.

Calcium release is required for the reorganization of the FMA and associated germ plasm

We tested whether inhibition of calcium release phenocopies the germ plasm segregation and FMA reorganization defects observed in *nebel* mutants, visualizing germ plasm RNPs with antibodies against serine 19 phospho-myosin light chain (P-myosin) (Nair et al., 2013), colabeled for microtubules, or by *in situ* hybridization to detect the RNA for *dead end* (*dnd*) (Weidinger et al., 2003) (Fig. 5). In wild-type embryos, germ plasm RNPs exhibit distal compaction, involving the transition from a rod-like structure along the forming furrow to a compacted mass at its distal end (Pelegri et al., 1999; Eno and Pelegri, 2013; reviewed by Eno and Pelegri, 2016) (Fig. 5A,K), which is coupled to the outward tilting and distal enrichment of associated FMA (Jesuthasan, 1998; Pelegri et al., 1999; Urven et al., 2006). In *nebel* mutants, germ plasm RNPs become recruited normally along the furrow and the resulting aggregate typically transitions into a more compact mass, but this mass and associated FMA fail to become enriched in distal furrow

Development (2018) 145, dev156604. doi:10.1242/dev.156604

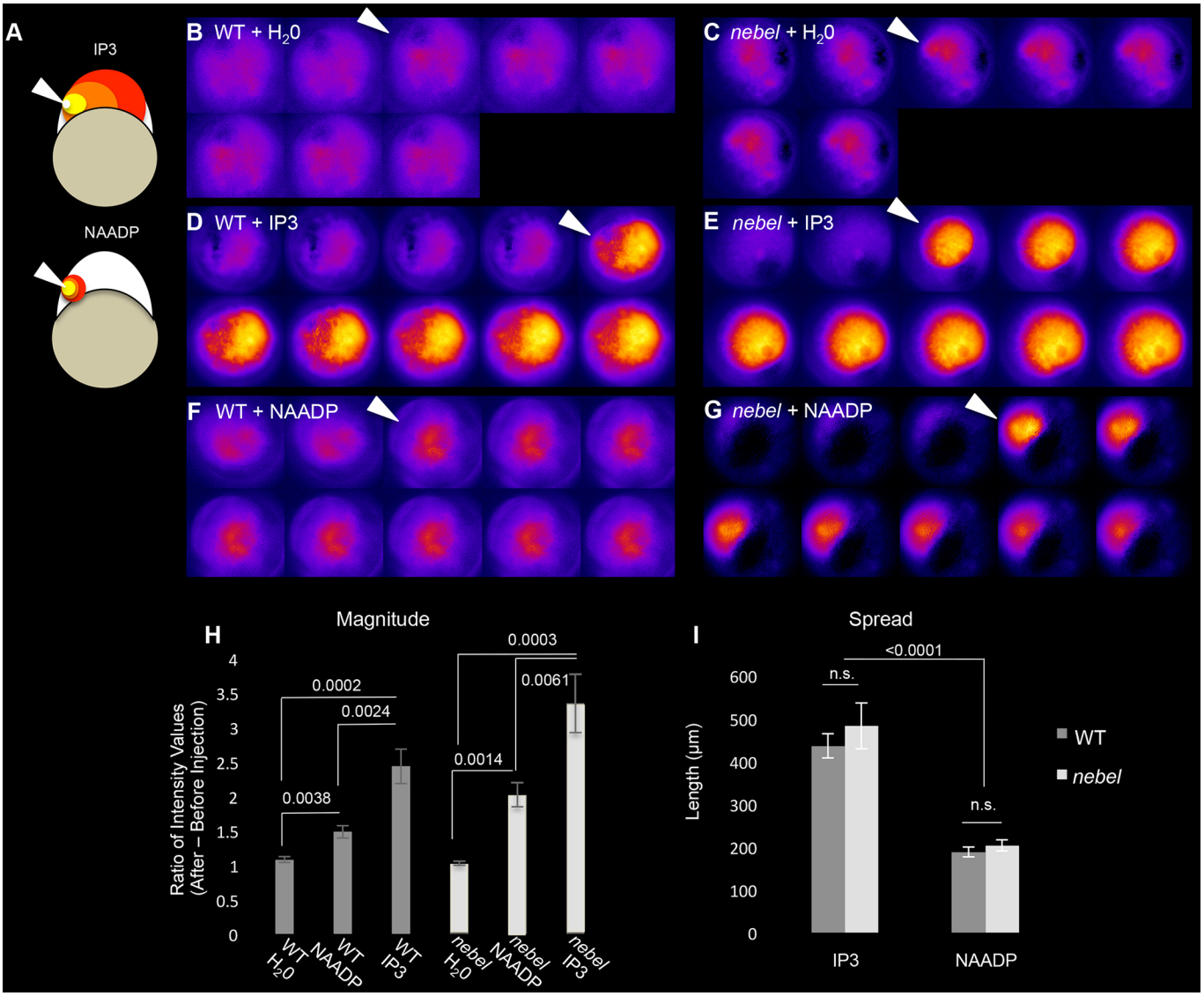

Fig. 3. *nebel* mutants exhibit a normal response to calcium release agonists. (A) Experimental design. (B-G) IP_3 or NAADP triggers a normal calcium release response in *nebel* mutants as compared with wild type. Agonist injection (arrowhead) was at 15-30 mpf, with time relative to injection indicated in min:s. (H,I) Quantification of magnitude and spatial extent of calcium release. Error bars indicate s.e.m. *P*-values according to paired *t*-test.

regions (Pelegri et al., 1999) (Fig. 5C,M). As expected considering the role of calcium in furrow initiation (Chang and Meng, 1995), inhibition of calcium release with an injection of the calcium chelator BAPTA results in a reduction in both furrow formation and germ plasm RNP furrow recruitment (Fig. 5E,O).

We next tested the effects on germ plasm and associated FMA in wild-type embryos of inhibitors predicted to interfere with SCWs (Lee et al., 2003). Exposure to the IP_3-mediated calcium release inhibitors 2-APB [an IP_3 receptor inhibitor (Bilmen and Michelangeli, 2002)] (Fig. 5G,Q) and U73122 [a Phospholipase C inhibitor that reduces IP_3 production (Macmillan and Mccarron, 2010)] (Fig. 5I,S) resulted in germ plasm RNPs and associated FMA retaining an arrangement characteristic of initiating furrows, namely a distribution of RNPs along the furrow without subsequent compaction, and an FMA perpendicular to the furrow without tilting or distal enrichment. Similar effects on RNPs and FMA were observed after exposure to the mitochondrial respiratory Complex II inhibitor 3-NP (Fig. 5B,L). Thus, treatments that interfere with SCWs in wild-type embryos lead to defects in enrichment at the distal furrow of germ plasm RNPs and associated FMA – effects similar to those observed in *nebel* mutants.

We further investigated FMA dynamics in live embryos under conditions that inhibit SCW formation using EMTB::EGFP transgenic fish (Fig. 6). In wild-type embryos at the 2- to 4-cell stage, the FMA translocates distally during furrow formation, where it subsequently undergoes disassembly (9 of 10 embryos, Fig. 6A) (Jesuthasan, 1998; Pelegri et al., 1999; Urven et al., 2006; Eno et al., 2016). By contrast, in *nebel* mutant embryos the FMA becomes enriched in the medial regions of the furrow, either at a single site at the center of the blastodisc (3 of 10 embryos, Fig. 6B) or at two sites abutting the center of the blastodisc (6 of 10 embryos, not shown) (see also Pelegri et al., 1999). Similar to our observations in fixed embryos, in live embryos in which IP_3 receptors are inhibited with 2-APB the FMA fails to become enriched in distal furrow regions, remaining instead in its original conformation along the length of the furrow (Fig. 6C). Similar effects are observed in live embryos after inhibition of mitochondrial function with the Complex II inhibitor 3-NP (data not shown).

Development (2018) 145, dev156604. doi:10.1242/dev.156604

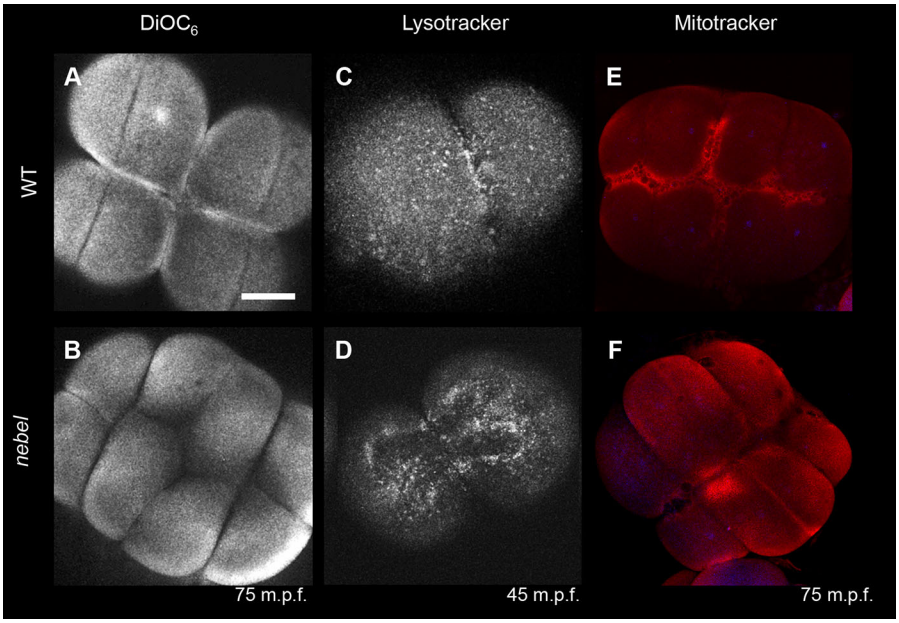

Fig. 4. Calcium stores are not properly enriched at the furrows in *nebel* mutants. Furrow enrichment of (A,B) ER (5/5 wild type, 0/9 *nebel* mutant), (C,D) lysosomes (6/6 wild type, 2/7 *nebel* mutant) and (E,F) mitochondria (13/14 wild type, 2/18 *nebel*). Images are from live (A-D) and fixed (E,F) embryos. Scale bar: 100 µm in A for A-F.

Furrow-associated SCWs are detected in early zebrafish embryos during the earliest cell cycles, leading to the 8-cell stage, but become undetectable during subsequent cell cycles (Chang and Meng, 1995). Such later cell cycles (leading to the 16-cell through 500-cell stages) continue to exhibit an FMA-like structure during early stages of cytokinesis. However, bundling of FMA tubules in wild type at these later stages occurs in medial regions of the furrow (Fig. 6D,E), similar to the behavior of coalescing midbodies in most cell types (Otegui et al., 2005; Steigemann and Gerlich, 2009). Thus, the presence of furrow-associated SCWs in the early wild-type embryo correlates with distally oriented reorganization of the FMA and associated germ plasm RNPs.

FMA reorganization mirrors the medial-to-distal polarity of SCWs

The requirement for intracellular calcium to implement the medial-to-distal reorganization of the FMA and germ plasm RNP aggregation is consistent with previous suggestions that SCWs originate in the center of the furrow and propagate towards its distal ends during furrow maturation (Chang and Meng, 1995; Webb et al., 1997; Créton et al., 1998), which we confirm using a transgenic line carrying the intracellular calcium reporter construct *Tg[βactin2:GCaMP6s]* (Chen et al., 2017) (Fig. 7A, Fig. S3A,G). Analysis of microtubules in live wild-type embryos using the EMTB::EGFP transgene shows that the distally oriented calcium increase is mirrored by an increase in FMA intensity in distal regions at later stages of furrow formation (Fig. 7C, Fig. S3C,K). By contrast, similar analyses in *nebel* mutant embryos show a lack of enrichment in the distal furrow for both intracellular calcium (Fig. 7B, Fig. S3B,H) and microtubules (Fig. 7D, Fig. S3D,L). Inhibition of SCWs in wild-type embryos using either the IP_3 receptor inhibitor 2-APB (Fig. S3E,I,M) or the mitochondrial activity inhibitor 3-NP (Fig. S3F,J,N) also interferes with the distal enrichment of both intracellular calcium and FMA. These analyses provide further support for a medial-to-distal directionality of SCWs, and show that it is associated with the distally oriented reorganization of the FMA and germ plasm RNP aggregates during furrow formation.

Calmodulin function and actomyosin dynamics are required for germ plasm RNP and FMA distal enrichment

Our studies suggest that SCWs convey information to polarize the cytoskeleton during furrow formation. We therefore considered as potential mediators of furrow polarization two factors whose activity is known to be calcium dependent: non-muscle myosin (Scholey et al., 1980) and Calmodulin (Albert et al., 1984; Clapham, 2007). Treatment with either of two Calmodulin inhibitors, W7 and W5, results in the FMA failing to undergo distal reorganization and in RNP aggregates remaining distributed along medial regions of the furrow (Fig. 5D,N; data not shown). Labeling of wild-type embryos with anti-Calmodulin and anti-Calmodulin kinase (CamK) antibodies shows enrichment of these proteins at the furrow in wild-type embryos (Fig. 8A,C). Furrow localization for both factors is reduced in *nebel* mutant embryos or 2-APB-treated embryos (Fig. 8B,D; data not shown), in which SCWs are inhibited. Inhibition of Rho activity by exposure to C3 exoenzyme also results in defects in RNP distal compaction (Fig. S4), as recently reported (Miranda-Rodríguez et al., 2017).

As previously reported (Urven et al., 2006), treatment of wild-type embryos with inhibitors of myosin activity, such as blebbistatin and ML7, results in a lack of FMA reorganization and germ plasm RNP distal compaction during furrow formation (Fig. 5F,H,P,R). Moreover, germ plasm RNPs are labeled with the P-myosin antibody (Nair et al., 2013), consistent with active myosin as one of their components. In contrast to Calmodulin and CamK, however, anti-P-myosin labeling is not reduced under conditions in which calcium is strongly reduced, as is also the case in *nebel* mutants (Fig. 5C′) or in wild-type embryos treated with inhibitors of IP_3 release (2-APB, U73122; Fig. 5G′,I′) or of mitochondrial activity (3-NP; Fig. 5B′) (see Discussion). Treatment of wild-type embryos with phalloidin indicates that stabilization of furrow F-actin also interferes with the distal movement of germ plasm RNPs (Fig. 5J,T).

Three-dimensional reconstructions show that, in control wild-type embryos, F-actin in the contractile ring forms indentations (Fig. 9A, inset), which during furrow maturation are progressively found in a more distal location, mirroring the enrichment of RNPs during distal compaction (Fig. 9B, bracket) (see Eno and Pelegri, 2018). In *nebel* mutants, in which germ plasm RNPs become recruited normally to the furrow (Fig. 9C) but remain in medial regions of the furrow after

Development (2018) 145, dev156604. doi:10.1242/dev.156604

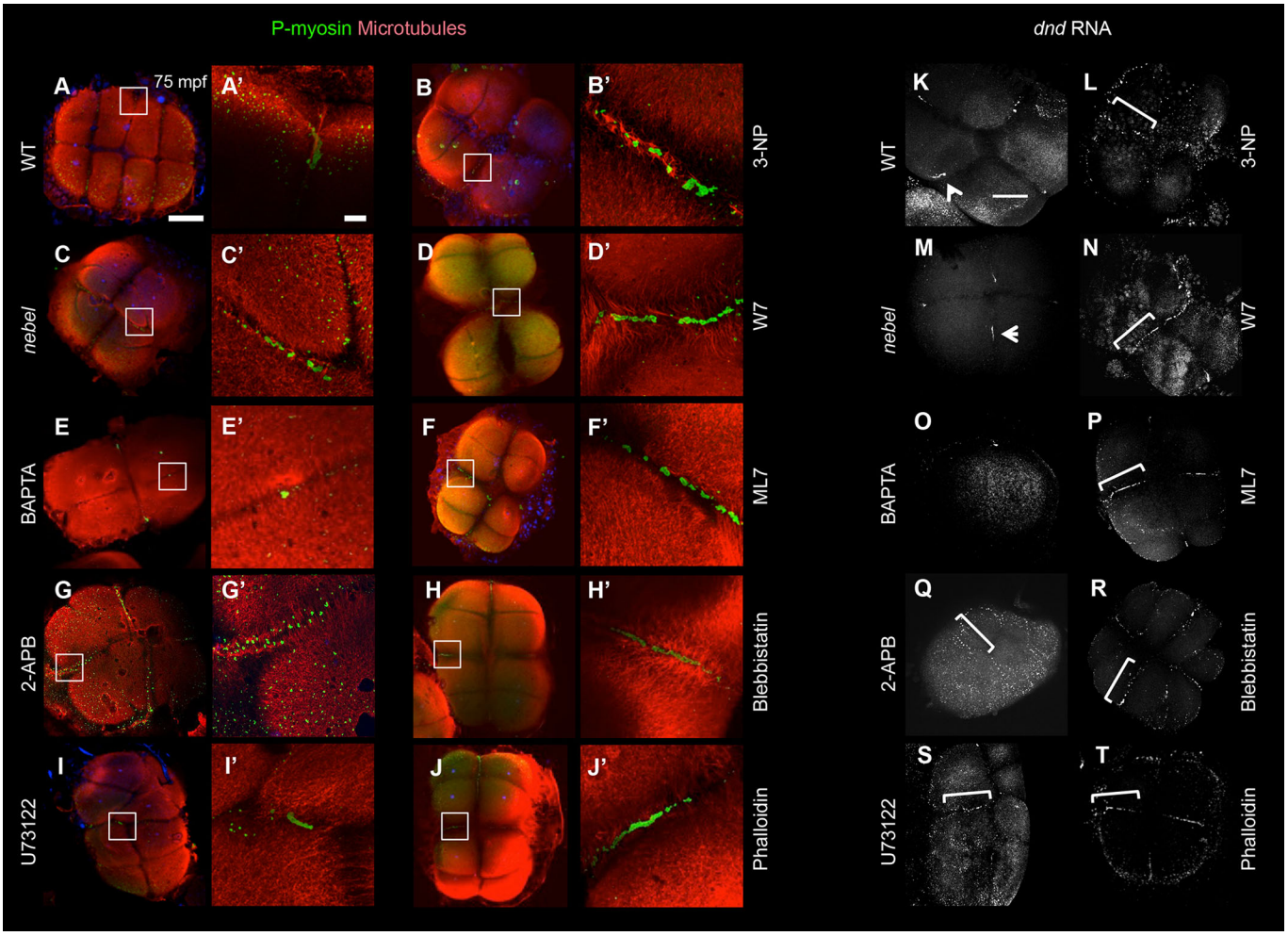

Fig. 5. Perturbation of calcium release inhibits germ plasm distal compaction. (A-J) RNPs labeled with anti-P-myosin and colabeled for microtubules. (A) In wild type, RNPs have underdone distal compaction in furrows for the first and second cell cycle (11/14 furrows). (C) In *nebel* mutants, RNPs fail to become distally enriched (2/15). (E) Injection after furrow initiation (35 mpf) of the calcium chelator BAPTA results in reduced and medially located RNPs (0/10). (B,D,F-J) Various inhibitors result in normal RNP furrow recruitment but aberrant RNP and FMA reorganization. (B) Mitochondrial activity inhibitor 3-NP (1/9). (D) Calmodulin inhibitors W7 (2/12) and W5 (not shown, 2/5). (F,H) Myosin light chain kinase inhibitor ML7 (F, 6/12) and active phospho-myosin inhibitor blebbistatin (H, 4/10). (G,I) IP_3 receptor inhibitor 2-APB (G, 0/9) and Phospholipase C inhibitor U73122 (I, 2/13). (J) F-actin dynamics inhibitor phalloidin (5/11). Boxed regions in A-J are magnified in A′-J′. (K-T) RNPs detected by *in situ* hybridization for *dnd* RNA. (K,M) Germ plasm undergoes compaction in distal furrow regions in wild type (K, arrowhead; 31/34) but not in *nebel* mutants (M, arrowhead; 1/19), where compaction occurs in medial furrow regions. (O) BAPTA (0/20 normal). Other inhibitors result in defects in distal compaction, with germ plasm instead retaining an elongated structure (bracket): 2-APB (Q, 0/7), U73122 (S, 0/5), 3-NP (L, 0/9), W7 (N, 1/11) and W5 (not shown, 3/10), ML7 (P, 2/10), blebbistatin (R, 3/11) and phalloidin (T, 1/13). In all cases, the fraction is normally distally compacted germ plasm/total number furrows examined. Scale bars: 100 µm in A for A-J and in K for K-T; 10 µm in A′ for A′-J′.

maturation (Fig. 9D, bracket), furrow F-actin indentations appear to be reduced (Fig. 9C, inset). Inhibition of calcium release by treatment of wild-type embryos with 2-APB also results in reduced furrow F-actin indentations (Fig. 9E, inset) and aberrant distal RNP enrichment (Fig. 9F, bracket). Similar effects are observed in embryos treated with Calmodulin or myosin inhibitors (Fig. 9G,I, insets; Fig. 9H,J, brackets). F-actin indentations continue to be apparent in phalloidin-treated embryos in spite of defects in germ plasm RNP distal movement (Fig. 9K-L′).

Altogether, these results and the accompanying manuscript (Eno and Pelegri, 2018) indicate that calcium- and myosin-dependent contractility, as well as F-actin dynamics, are essential for the distal reorganization of germ plasm RNPs and associated FMA.

DISCUSSION

In this study, we show that *nebel* mutants exhibit changes in furrow-associated SCWs, specifically a reduction in calcium release levels and an increase in release frequency. Our studies show that directional calcium release during the early mitotic cell cycles has a key role in the reorganization of furrow-associated microtubules and associated RNPs in the early embryo, leading to their enrichment at the furrow distal ends.

nebel-dependent furrow enrichment of calcium stores is required for SCW formation

Wild-type embryos exhibit two primary SCW waves: an initiation wave prior to furrow indentation and a deeper and more intense wave during furrow maturation (Chang and Meng, 1995; Reinhard et al., 1995; Webb et al., 1997; Créton et al., 1998). By contrast, *nebel* mutants exhibit SCWs of comparatively low intensity. Intracellular calcium release is essential for both furrow initiation and maturation (Lee et al., 2003), but *nebel* mutant embryos are, in most cases, able to initiate furrow ingression (Pelegri et al., 1999; this report). These observations suggest that reduced SCWs in *nebel* mutants are sufficient for furrow initiation but not furrow maturation.

Development (2018) 145, dev156604. doi:10.1242/dev.156604

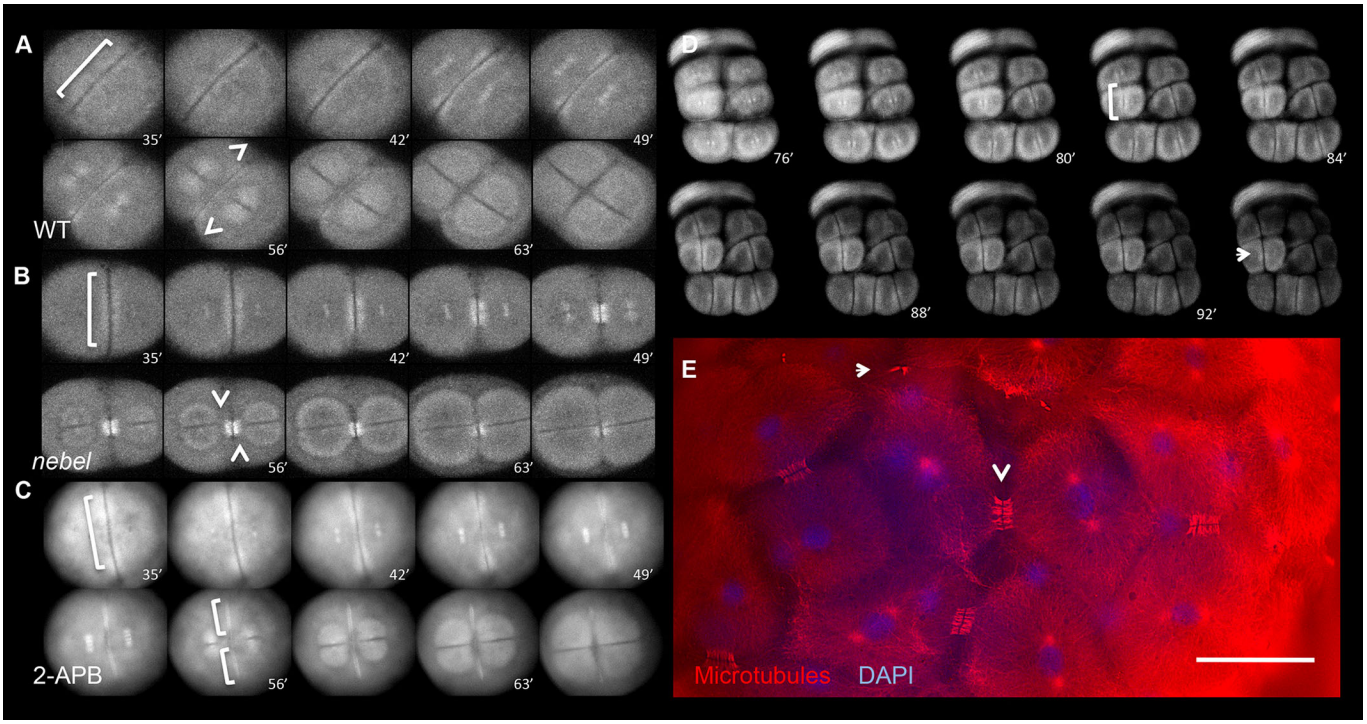

Fig. 6. The FMA acts as a calcium-dependent modified midbody. (A-D) EMTB::EGFP transgenic fish. In wild type (A), the FMA initially aligns along the furrow (brackets) and becomes enriched distally (arrowheads). In *nebel* mutants (B), the FMA is initially normal but bundles in medial furrow regions. In 2-APB-treated wild-type embryos (C), the FMA forms normally but remains aligned along the furrow. During the early cleavage stages of wild-type EMTB::EGFP embryos (D), the FMA forms (bracket) but bundles medially (arrow). Time is in min. (E) Fixed wild-type 64-cell embryos stained for microtubules and for DNA (DAPI), showing inwardly bundling FMAs (arrowhead) and remnants (arrow). Scale bar: 75 µm in E.

The calcium release response after injection of IP_3 and NAADP receptor antagonists is robust in *nebel* mutants, indicating that calcium stores are present in the embryos and that IP_3 and NAADP receptors are functional. However, *nebel* embryos show defects in the localization of calcium stores such as the ER and lysosomes (which contain IP_3 and NAADP receptors, respectively). In wild type, these calcium-rich organelles are enriched in the forming furrows, whereas in *nebel* embryos they are distributed throughout the blastomeres. We also find that *nebel* embryos lack furrow enrichment of mitochondria, another organelle involved in calcium release and buffering (see below). Segregation analysis shows that *nebel* is located between markers z21679 and z14228 on chromosome 3 (our unpublished data), and we are currently attempting to unambiguously identify the affected gene and determine its molecular function.

Precise patterns of calcium release are known to depend on multiple cellular calcium stores often interacting in close proximity (Penny et al., 2015). Thus, it is likely that reduced proximity and density of calcium stores at the furrow results in the observed changes in SCWs of *nebel* mutants (Fig. 10A). Our results highlight the importance of the spatial enrichment of calcium stores for the generation of SCWs.

Furrow mitochondria contribute to SCW dynamics

Previous studies have shown that the oocyte cortex exhibits autocatalytic properties characteristic of an excitable medium, where IP_3-dependent calcium release above an activation threshold results in further calcium release through calcium-induced calcium release (CICR) (Lechleiter and Clapham, 1992). In addition, calcium release channels are repressed by high concentrations of calcium, creating a negative-feedback loop. Together, CICR and calcium-mediated channel inhibition are thought to mediate the spatial and temporal progression of calcium waves (Chang and Meng, 1995; Reinhard et al., 1995; Webb et al., 1997; Créton et al., 1998).

Mitochondria also accumulate and release calcium (DeLuca and Engstrom, 1961; Ichas et al., 1997). Calcium uptake into mitochondria is coupled to the proton electrochemical gradient across its inner membrane (Gunter and Pfeiffer, 1990) and raises the calcium concentration threshold for CICR excitation, resulting in calcium waves of higher amplitude and decreased frequency (Jouaville et al., 1995). Conversely, a decrease in mitochondrial activity results in calcium waves of reduced amplitude and increased frequency, as observed in *nebel* mutants.

Because of the low sensitivity of mitochondria to calcium concentrations, the action of mitochondria has been proposed to rely strongly on the close proximity of mitochondria to IP_3-dependent receptors in the ER (Jouaville et al., 1995). Thus, the defective furrow enrichment of mitochondria is also likely to contribute to the SCW defects in *nebel* mutants.

Calcium-dependent FMA reorganization allows distal enrichment of associated germ plasm RNPs

The FMA in early vertebrate embryos such as *Xenopus* and zebrafish has been proposed to be homologous to the midbody (Danilchik et al., 1998; Jesuthasan, 1998), a microtubule-based structure found in other cell types essential for membrane abscission during the final stages of cytokinesis (Skop et al., 2004). Reorganization of the canonical midbody involves the entire set of midzone microtubules undergoing inward bundling, towards the center of the dividing cell (reviewed by Mierzwa and Gerlich, 2014). By contrast, the FMA in early zebrafish embryos undergoes

Development (2018) 145, dev156604. doi:10.1242/dev.156604

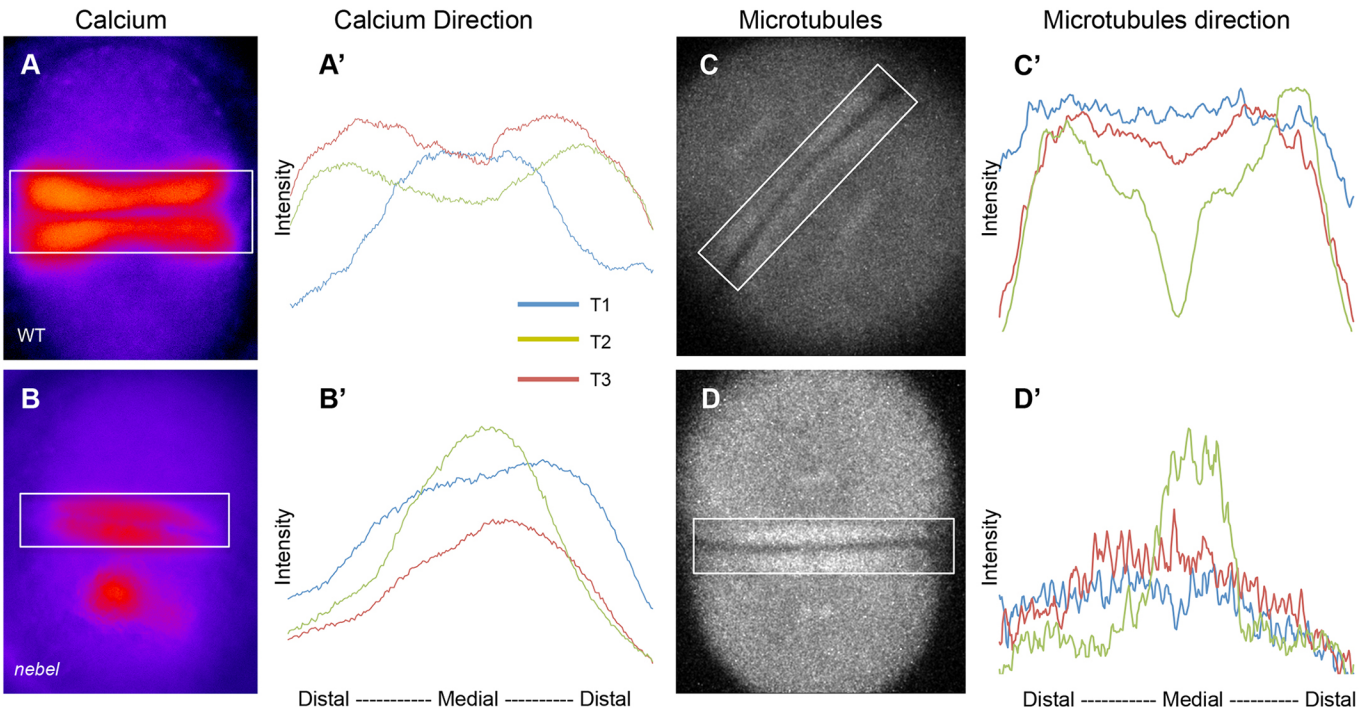

Fig. 7. FMA distal enrichment correlates with SCW directionality. (A-B′) Calcium levels in single *Tg[βactin2:GCaMP6s]* transgenic embryos during furrow progression, with plotted profiles (A′,B′) corresponding to boxed areas. Wild-type embryos (A′), but not *nebel* mutants (B′), show increasing distal calcium levels. (C-D′) Microtubules in EMTB::EGFP transgenic embryos during furrow progression (C,D), with plotted profiles (C′,D′). Wild-type embryos (C′), but not *nebel* mutants (D′), show distal enrichment. Time points T1, T2 and T3 correspond, respectively, to frames within one-tenth of the total sequence of acquired images spanning a furrow formation cycle at the beginning, middle and end of that cycle. See Fig. S4 for additional profiles.

bundling of two populations, each representing half of its tubules, towards the distal furrow ends. We find that, in embryos with reduced SCWs, the FMA fails to undergo distally oriented bundling. An inwardly bundling FMA, resulting in a single medial structure, is also observed in wild-type blastomeres at later stages of development, when furrows are no longer associated with SCWs. These observations, together with the medial-to-distal directionality of SCWs along the furrow (Chang and Meng, 1995; Webb et al., 1997; Créton et al., 1998; this study), suggest a role for SCWs in modifying the FMA, a structure observed in large cells that is analogous to the midbody, into two distally bundling structures (Fig. 10B). The distal FMA enrichment is coupled to the formation of large germ plasm masses at the furrow distal ends.

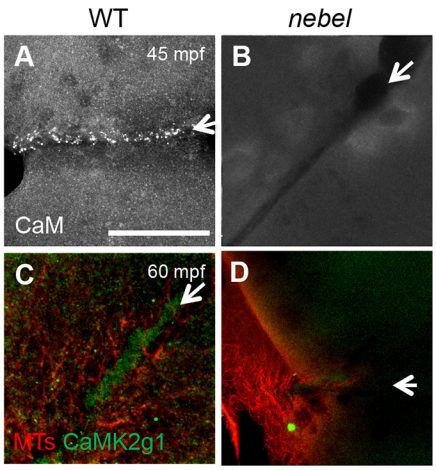

Fig. 8. Calmodulin/CaMK is recruited to the furrow in wild-type but not in *nebel* embryos. Wild-type furrows show localization of Calmodulin (A, 5/7) and CaMK (CaMK2γ1; C, 13/15). *nebel* mutants lack this localization (B, 0/15; D, 0/10). Arrows indicate furrows. Scale bars: 10 µm in A for A-D.

Germ plasm has been found to aggregate at cleavage furrows in other vertebrates, such as in the chick embryo (Tsunekawas et al., 2000). In *Xenopus*, germ plasm also shows an association to furrow ends (Whittington and Dixon, 1975). Pluripotency shares common features with the germ cell state, such as a Blimp-1-positive stage (reviewed by Welling and Geijsen, 2013), and is associated with midbody inheritance (Ettinger et al., 2011; Kuo et al., 2011). Thus, studies on germ plasm segregation in zebrafish might provide valuable clues to aid in understanding the segregation during cell division of cell fate determinants associated with midbody-like structures.

Mechanism of germ plasm distal compaction

Germ plasm RNP segregation during furrow formation involves not only the reorganization of the germ plasm aggregate itself but also the reorganization of associated microtubule and F-actin networks (Fig. 10C) (see also Eno and Pelegri, 2018). Medial-to-distal SCW directionality is associated with the observed distally directed reorganization, suggesting that the direction of calcium release itself constitutes a polarizing cue along the furrow. SCWs are associated with the localization to the furrow of Calmodulin and its potential downstream regulators such as CamK (this report) and Rho (Miranda-Rodríguez et al., 2017; this report), enrichments that are likely to rely on the presence of binding partners and which are thought to allow subcellular functional specificity (Lloyd-Burton et al., 2007; Bielak-Zmijewska et al., 2008; Fok et al., 2008; Mikl et al., 2011; Abe et al., 2012; Liu and Murray, 2012; Braun and Olayioye, 2015).

SCWs could provide a directional cue along the furrow by acting directly on F-actin. A potential candidate effector to mediate

Development (2018) 145, dev156604. doi:10.1242/dev.156604

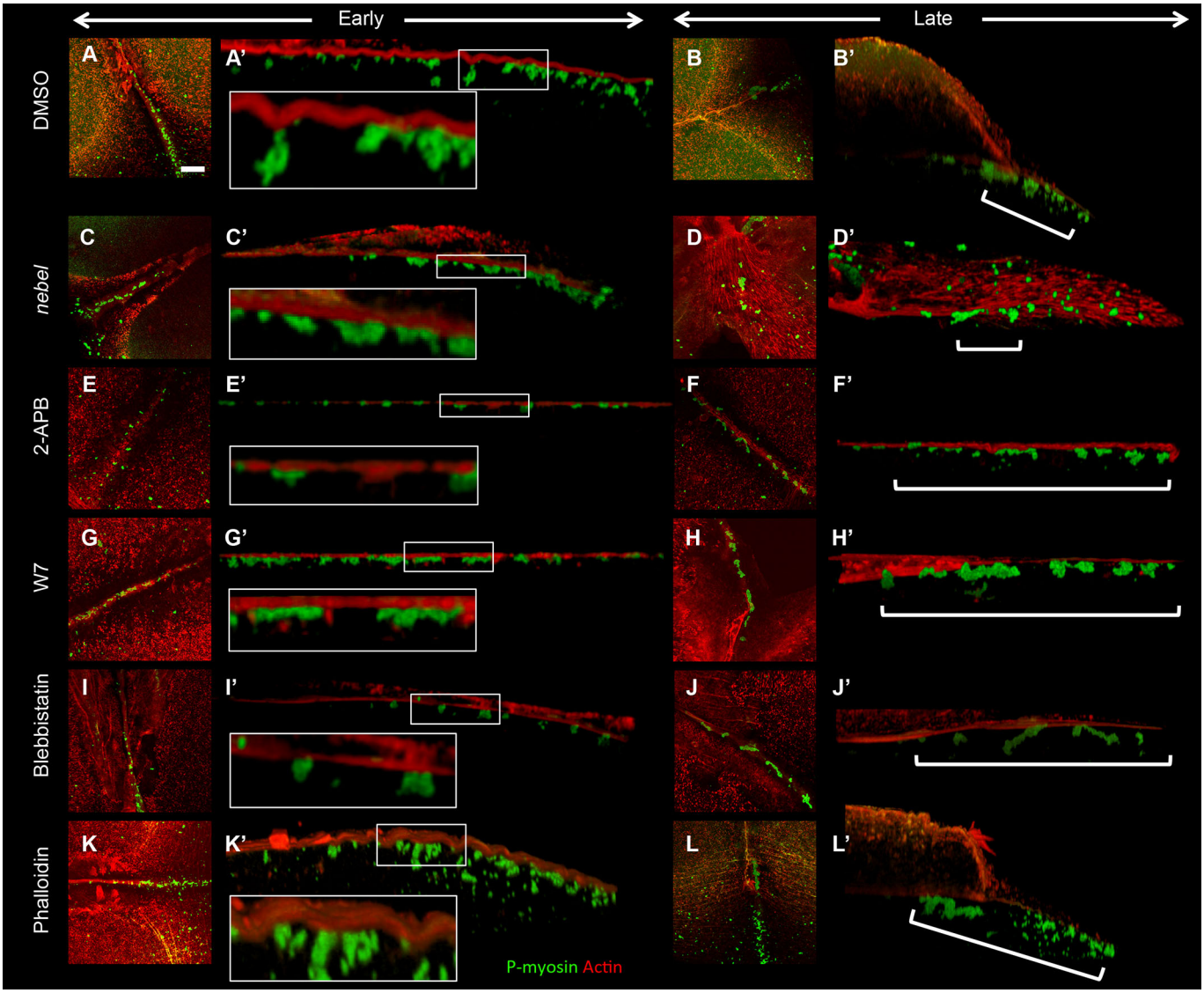

Fig. 9. Furrow F-actin contractions associated with germ plasm RNPs depend on calcium, Calmodulin and myosin. (A-L) *z*-projections from early and late furrows (second and first furrows at 60 mpf, respectively). (A′-L′) Lateral views showing F-actin contractions and RNPs. Control treated embryos exhibit F-actin indentations (A,A′, 5/7) and subsequent RNP distal enrichment (B,B′, 4/5). *nebel* mutants and 2-APB-treated wild-type embryos exhibit reduced F-actin contractions (C,C′, 2/10) and failed distal RNP enrichment (D,D′, 3/10). (E-J) Various inhibitors result in reduced F-actin indentations and RNP distal enrichment: IP_3 receptor inhibitor 2-APB (E-F′, 1/5, 0/4); Calmodulin inhibitor W7 (G-H′, 0/4, 0/4); myosin inhibitor blebbistatin (I-J′, 2/5, 2/7). Phalloidin-treated embryos exhibit F-actin indentations (K,K′, 5/8) but late furrows exhibit incomplete RNP distal enrichment (L,L′, 0/14). Insets (A′,C′,E′,G′,I′,K′) are magnifications of the boxed regions. Brackets (B′,D′,F′,H′,J′,L′) highlight regions of RNP distribution. Scale bar: 10 µm in A for A-L.

the effects of SCWs is non-muscle myosin II (reviewed by Conti and Adelstein, 2008). Our previous studies demonstrated a requirement for myosin function in distal compaction (Urven et al., 2006), and we determine that furrow F-actin indentations, associated with aggregating RNPs, depend on myosin activity. Antibodies that recognize the serine 19 phosphorylated form of myosin light chain, diagnostic of myosin-II activation (Ikebe and Hartshorne, 1985), label aggregating germ plasm RNPs (Nair et al., 2013). However, P-myosin labeling in RNPs remains at apparently normal levels in *nebel* mutants or calcium-inhibited wild-type embryos, indicating that this particular phosphorylation is unlikely on its own to mediate a directional response to SCWs. It is possible that SCWs, via Calmodulin, directly influence the F-actin cytoskeleton network, for example through the action of the Rho and ROCK pathway (Wolff et al., 1999; Harada et al., 2000; Fransson et al., 2003; Okabe et al., 2003; Miranda-Rodríguez et al., 2017; this report) or other Calmodulin mediators (Zhang et al., 2012; Zhao et al., 2012).

Directional reorganization may also be mediated by directional bundling of FMA tubules through processes analogous to those occurring during midbody formation in smaller cell types (Mierzwa and Gerlich, 2014), and indeed the integrity of FMA microtubules is important for the distal aggregation of RNPs (Pelegri et al., 1999). In neuronal synapses, activation of CamK by intracellular calcium promotes microtubule stabilization and bundling through the regulation of microtubule-associated proteins (MAPs) (reviewed by McVicker et al., 2015). It is possible that calcium may be similarly acting to promote distal stabilization of FMA tubules in the zebrafish embryo. Recent studies have shown a role for microtubule ends in promoting F-actin polymerization, by recruiting the mDia

Development (2018) 145, dev156604. doi:10.1242/dev.156604

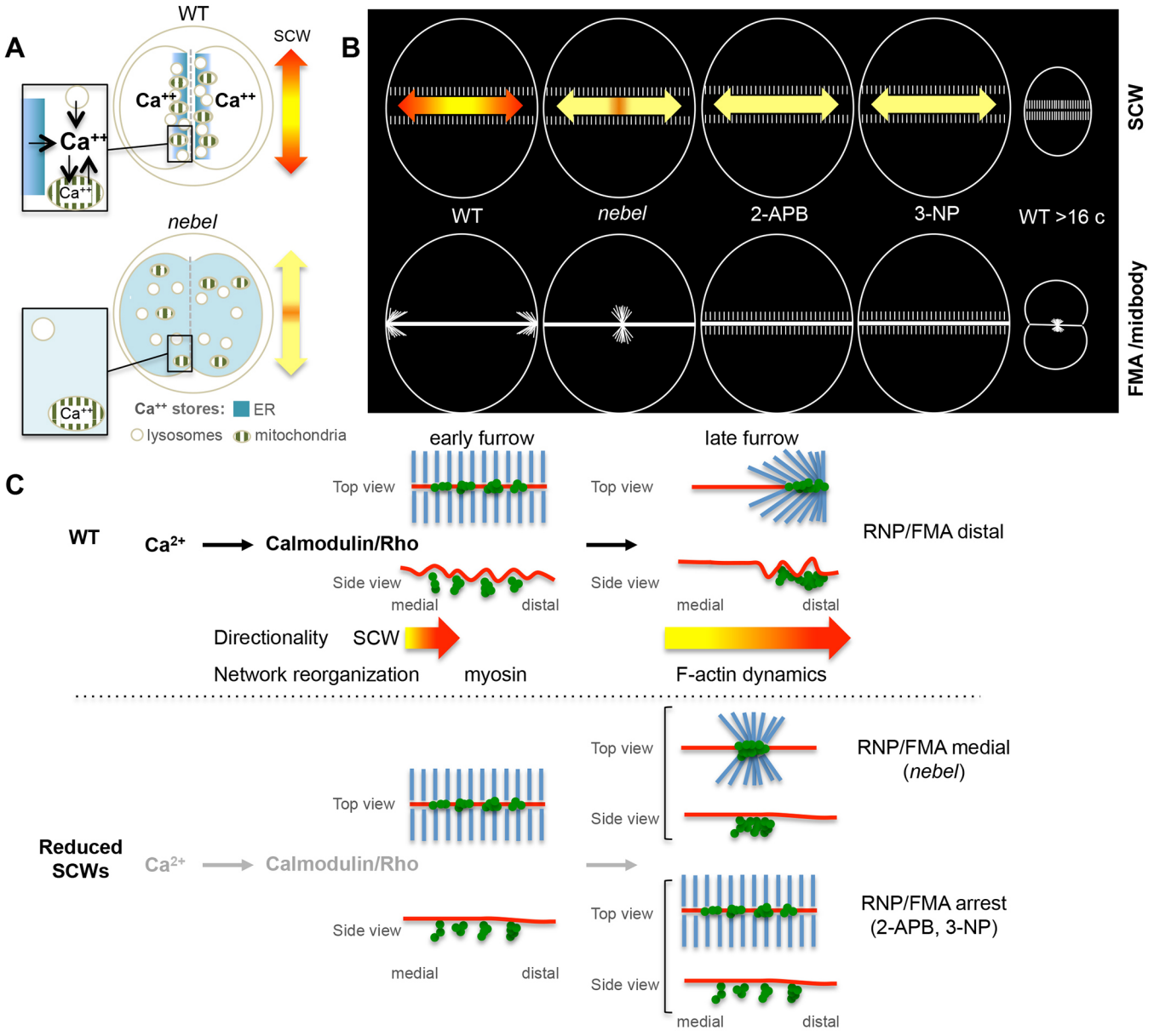

Fig. 10. SCWs confer medial-to-distal directionality. (A) In wild-type embryos, intracellular organelles functioning in calcium release (ER, lysosomes) or buffering (mitochondria) become enriched to the forming furrows, with their close proximity facilitating high cytosolic calcium concentrations to generate SCWs. In *nebel* mutants, calcium stores fail to become enriched at the furrow, resulting in defective SCWs. (B) In wild-type embryos, SCWs signal to split the FMA as two distinct distal entities. Reduction of SCWs in *nebel* mutants and calcium-inhibited embryos (IP_3 receptor inhibition by 2-APB; mitochondrial activity inhibition by 3-NP) results in medially enriched or arrested FMAs. Later, wild-type blastomeres lack SCWs and also form a single medial FMA. (C) Events leading to RNP distal aggregation, with early furrows at left and late furrows at right, top views highlighting RNPs and FMA, and side views RNPs and F-actin. SCWs are proposed to impart directional cytoskeletal reorganization that facilitates RNP distal compaction. This reorganization additionally depends on myosin II function and F-actin dynamics (Urven et al., 2006; Eno and Pelegri, 2018).

formins (McVicker et al., 2015; Henty-Ridilla et al., 2016), and it will be interesting to test a potential role for the FMA in modulating F-actin dynamics.

Zebrafish germ plasm RNPs are thought to interact via fluid phase properties mediated by intrinsically disordered proteins (Brangwynne et al., 2009, 2015), such as Bucky ball (Marlow and Mullins, 2008; Bontems et al., 2009; Heim et al., 2014; Riemer et al., 2015; Boke et al., 2016). It is possible that such forces also contribute to RNP reorganization and multimerization during furrow formation. Indeed, the transition of RNP aggregate arrangement from an elongated rod to a compact mass during furrow maturation is expected to involve an overall increase in RNP neighbor-neighbor interactions, presumably towards a reduced energy state. The observation that germ plasm RNPs undergo compaction, albeit in medial regions, in embryos in which the microtubule network has been reduced through nocodazole treatment (Pelegri et al., 1999) further supports an intrinsic ability of RNPs to undergo reorganization through inter-particle interactions.

Understanding the precise molecular mechanisms underlying this complex process, involving cellular mediator signals, F-actin, microtubules and RNPs, will provide insights into how organelles exhibiting fluid phase behavior reorganize in the context of complex networks.

Development (2018) 145, dev156604. doi:10.1242/dev.156604

In summary, we show that SCWs contribute to overriding the normal tendency of microtubules during late cytokinesis to bundle as a single unit in the center region of the furrow, facilitating instead the formation of two half-midbody equivalents, one at each of the distal furrow ends. This cytoskeletal reorganization allows the generation of multiple large germ plasm masses, each capable of inducing the primordial germ cell fate. Our studies provide insights into how processes related to the cell division machinery can be modified by overlying cellular signals to facilitate the directed segregation of cellular determinants.

MATERIALS AND METHODS

Fish maintenance

Stocks of wild-type AB and *nebel* (*neb*^{t023}) mutant (Pelegri et al., 1999, 2004; Pelegri and Schulte-Merker, 1999) lines were raised and maintained under standard conditions at 28.5°C (Brand et al., 2002). Homozygous mutant *nebel* fish were identified by genotyping flanking SSLP markers z21679 and z14228. End-point genotyping (Integrated DNA Technologies) was used to maintain the line with custom-designed primers and probes (Table S1). Mutant embryos were obtained by crossing homozygous *nebel* females to AB males. Embryos were collected and allowed to develop in E3 embryonic medium (Pelegri and Schulte-Merker, 1999) and were staged according to time to egg activation/fertilization and standard morphological landmarks (Kimmel et al., 1995). Embryos in all experiments were at 26°C, with the exception of embryos for the morphological analysis of furrow initiation and completion, which were transferred within several minutes after fertilization to 22°C to increase phenotypic penetrance (Pelegri et al., 1999). Activated eggs were obtained through exposure of mature, extruded eggs to E3 medium in the absence of sperm.

Imaging with calcium-sensitive dyes

Analysis with calcium-sensitive dyes was performed by injecting either the ratiometric calcium-sensitive dye Fura-2-Dextran (Slusarski et al., 1997; Westfall et al., 2003) or the calcium indicator Oregon Green 488 BAPTA-Dextran (OGB) (Thermo Fisher O6812) at the 1-cell stage, followed by imaging and analysis. For Fura-2-Dextran, embryos were microinjected with ∼3 nl Fura-2-Dextran solution (Molecular Probes B6810), oriented in a glass-bottomed dish on a Zeiss Axiovert, and image pairs at 340 nm and 380 nm excitation wavelengths (510 nm emission) were collected at 15 s intervals, for a total of 300 image pairs. The ratio image – a pixel-by-pixel match of both excitation wavelengths – was calculated using Ratio Tool (Innovision) software. For OGB, embryos were injected with a mixture of 100 µM OGB and 40 µM Rhodamine (Ashworth et al., 2001) and imaged using a Zeiss Axioplan2 epifluorescence microscope. Embryos were imaged for OGB and Rhodamine at one focal plane every 3 s. For each time point, the Rhodamine channel was subtracted from the OGB channel using FIJI. Kymograph and Plot Profile (FIJI) were used to obtain values for analysis of calcium pulses using AxoGraph software.

Drug exposure and agonist injection

Drug exposure was initiated by exposure of dechorionated embryos in E3 medium within 15 min of fertilization, with the exception of BAPTA, which was microinjected (∼1 nl at 5 mM; Sigma A1076) after furrow initiation at 35 minutes postfertilization (mpf) to avoid karyokinesis and/or furrow initiation defects (Chang and Meng, 1995). For drug exposure, inhibitor concentrations in E3 medium were: IP_3 receptor, 500 µM 2-APB (Sigma D9754); mitochondrial Complex I inhibitor, 100 µM rotenone (Sigma R8875); mitochondrial Complex II inhibitor, 10 mM 3-NP (Sigma N5636); Calmodulin, 400 µM W7 (Tocris 0369); Phospholipase (C), 100 µM U73122 (Tocris 1268); Rho, 20 µg/ml C3 exoenzyme (Calbiochem 341208). Control embryos were exposed to the same concentration of carrier solvent (DMSO).

For agonist injection into unfertilized eggs and embryos, solutions of IP_3 (Sigma I9766) and NAADP (Sigma N5655) were injected at 10 µM and 0.5 µM by 15 mpf in ∼0.25 nl. Injection of $CaCl_2$ (Sigma C1016) at 0.1 and 0.2 mM in ∼1 nl was carried out together with 0.1 M KCl to prevent egg damage (Gilmour et al., 2002), with controls injected with KCl alone at 0.2 mM.

In situ hybridization, immunofluorescence, fluorescence labeling and live imaging

In situ hybridizations were carried out as described previously (Eno and Pelegri, 2013) with digoxigenin-labeled probes for germ plasm RNAs *dnd* (*dnd1*) (Weidinger et al., 2003) and *vasa* (*ddx4*) (Yoon et al., 1997). Immunofluorescence was carried out as previously described (Lindeman and Pelegri, 2012; Eno et al., 2016) with primary antibodies against phospho-myosin light chain (S19) (Cell Signaling Technology 3671L, 1:50) (Nair et al., 2013), Calmodulin (Millipore 05-173, 1:50) and alpha-tubulin (Sigma T5168, 1:2500). Percentage RNP distal enrichment (compaction) was determined using the number of furrows at the appropriate stage of formation (1-4 furrows per embryo where RNPs are detected). Imaging was acquired using either an Axioplan2 epifluorescence microscope or a Zeiss LSM510 confocal microscope. All images were analyzed using FIJI.

Fluorescent dyes, diluted in E3 medium, were Lysotracker Red (Thermo Fisher L7528, 1:100), MitotrackerCMXRos (Thermo Fisher M7512, 1:100) and $DiOC_6$ (Thermo Fisher D273, 1:2500). Exposure to dyes was initiated by 15 mpf and dyes were washed out with several changes of E3 medium before imaging at 30 mpf. Transgenic lines to visualize microtubules and intracellular calcium were EMTB-EGFP (Wühr et al., 2010) and *Tg[βactin2:GCaMP6s]* (Chen et al., 2017), respectively. Live imaging employed an Axioplan2 epifluorescence microscope. Image processing and analysis were carried with FIJI modules Z-project (projections and 3D reconstructions), Reslice (kymographs) and Plot Profile (quantitation).

Acknowledgements

We thank members of our laboratories for advice during various stages of this work, as well as animal husbandry staff for the care of the aquatic facility. We thank Erica Weber for assistance with image acquisition. We are also grateful to Drs Liliana Solnica-Krezel (Washington University School of Medicine), Martin Wühr (Harvard University, Princeton University) and Tim Mitchison (Harvard University) for generously providing transgenic lines.

Competing interests

The authors declare no competing or financial interests.

Author contributions

Conceptualization: C.E., T.G., D.C.S., F.P.; Methodology: C.E., T.G., D.C.S.; Software: T.G., D.C.S.; Validation: C.E.; Formal analysis: C.E., T.G., D.C.S.; Investigation: C.E., D.C.S.; Writing - original draft: C.E.; Writing - review & editing: C.E., T.G., D.C.S., F.P.; Visualization: C.E.; Supervision: F.P.; Project administration: F.P.; Funding acquisition: C.E., F.P.

Funding

Funding was provided by National Institutes of Health grants to C.E. (F31GM108449), D.C.S. (CA112369) and F.P. (GM065303). Deposited in PMC for release after 12 months.

Supplementary information

Supplementary information available online at
http://dev.biologists.org/lookup/doi/10.1242/dev.156604.supplemental

References

Abe, M., Makino, A., Hullin-Matsuda, F., Kamijo, K., Ohno-Iwashita, Y., Hanada, K., Mizuno, H., Miyawaki, A. and Kobayashi, T. (2012). A role for sphingomyelin-rich lipid domains in the accumulation of phosphatidylinositol-4,5-bisphosphate to the cleavage furrow during cytokinesis. *Mol. Cell. Biol.* **32**, 1396-1407.

Albert, K. A., Wu, W. C., Nairn, A. C. and Greencard, P. (1984). Inhibition by calmodulin of calcium/phospholipid-dependent protein phosphorylation. *Proc. Natl. Acad. Sci. USA* **81**, 3622-3625.

Alston, T. A., Mela, L. and Bright, H. J. (1977). 3-Nitropropionate, the toxic substance of Indigofera, is a suicide inactivator of succinate dehydrogenase. *Proc. Natl. Acad. Sci. USA* **74**, 3767-3771.

Ashworth, R., Zimprich, F. and Bolsover, S. R. (2001). Buffering intracellular calcium disrupts motoneuron development in intact zebrafish embryos. *Dev. Brain Res.* **129**, 169-179.

Babcock, D. F., Herrington, J., Goodwin, P. C., Park, Y. B. and Hille, B. (1997). Mitochondrial participation in the intracellular Ca^{2+} network. *J. Cell Biol.* **136**, 833-844.
Berridge, M. J. (1993). Inositol trisphosphate and calcium signalling. *Nature* **361**, 315-325.
Berridge, M. J., Bootman, M. D. and Roderick, H. L. (2003). Calcium signalling: dynamics, homeostasis and remodelling. *Nat. Rev. Mol. Cell Biol.* **4**, 517-529.
Bielak-Zmijewska, A., Kolano, A., Szczepanska, K., Maleszewski, M. and Borsuk, E. (2008). Cdc42 protein acts upstream of IQGAP1 and regulates cytokinesis in mouse oocytes and embryos. *Dev. Biol.* **322**, 21-32.
Bilmen, J. G. and Michelangeli, F. (2002). Inhibition of the type 1 inositol 1,4,5-trisphosphate receptor by 2-aminoethoxydiphenylborate. *Cell. Signal.* **14**, 955-960.
Boke, E., Ruer, M., Wühr, M., Coughlin, M., Lemaitre, R., Gygi, S. P., Alberti, S., Drechsel, D., Hyman, A. A. and Mitchison, T. J. (2016). Amyloid-like self-assembly of a cellular compartment. *Cell* **166**, 637-650.
Bontems, F., Stein, A., Marlow, F., Lyautey, J., Gupta, T., Mullins, M. C. and Dosch, R. (2009). Bucky ball organizes germ plasm assembly in zebrafish. *Curr. Biol.* **19**, 414-422.
Braat, A. K., Zandbergen, T., van de Water, S., Goos, H. J. T. and Zivkovic, D. (1999). Characterization of zebrafish primordial germ cells: morphology and early distribution of vasa RNA. *Dev. Dyn.* **216**, 153-167.
Brand, M., Granato, M. and Nüsslein-Volhard, C. (2002). Keeping and raising zebrafish. In *Zebrafish - A Practical Approach*, Vol. 261 (ed. C. Nüsslein-Volhard and R. Dahm), pp. 7-37. Oxford: Oxford University Press.
Brangwynne, C. P., Eckmann, C. R., Courson, D. S., Rybarska, A., Hoege, C., Gharakhani, J., Jülicher, F. and Hyman, A. A. (2009). Germline P granules are liquid droplets that localize by controlled dissolution/condensation. *Science* **324**, 1729-1732.
Brangwynne, C. P., Tompa, P. and Pappu, R. V. (2015). Polymer physics of intracellular phase transitions. *Nat. Phys.* **11**, 899-904.
Braun, A. C. and Olayioye, M. A. (2015). Rho regulation: DLC proteins in space and time. *Cell. Signal.* **27**, 1643-1651.
Chang, D. C. and Meng, C. (1995). A localized elevation of cytosolic free calcium is associated with cytokinesis in the zebrafish embryo. *J. Cell Biol.* **131**, 1539-1545.
Chen, J., Xia, L., Bruchas, M. R. and Solnica-Krezel, L. (2017). Imaging early embryonic calcium activity with GCaMP6s transgenic zebrafish. *Dev. Biol.* **430**, 385-396.
Clapham, D. E. (2007). Calcium signaling. *Cell* **131**, 1047-1058.
Conti, M. A. and Adelstein, R. S. (2008). Nonmuscle myosin II moves in new directions. *J. Cell Sci.* **121**, 11-18.
Créton, R., Speksnijder, J. E. and Jaffe, L. F. (1998). Patterns of free calcium in zebrafish embryos. *J. Cell Sci.* **111**, 1613-1622.
Danilchik, M. V., Funk, W. C., Brown, E. E. and Larkin, K. (1998). Requirement for microtubules in new membrane formation during cytokinesis of *Xenopus* embryos. *Dev. Biol.* **194**, 47-60.
DeLuca, H. F. and Engstrom, G. W. (1961). Calcium uptake by rat kidney mitochondria. *Proc. Natl. Acad. Sci. USA* **47**, 1744-1750.
Eno, C. and Pelegri, F. (2013). Gradual recruitment and selective clearing generate germ plasm aggregates in the zebrafish embryo. *Bioarchitecture* **3**, 125-132.
Eno, C. and Pelegri, F. (2016). Germ cell determinant transmission, segregation and function in the zebrafish embryo. In *Insights from Animal Reproduction* (ed. R. P. Carreira), pp. 115-142. Rijeka, Croatia: InTech.
Eno, C. and Pelegri, F. (2018). Modulation of F-actin dynamics by maternal Mid1ip1l controls germ plasm aggregation and furrow recruitment in the zebrafish embryo. *Development* **145**, dev156596.
Eno, C., Solanki, B. and Pelegri, F. (2016). *aura* (*mid1ip1l*) regulates the cytoskeleton at the zebrafish egg-to-embryo transition. *Development* **143**, 1585-1599.
Ettinger, A. W., Wilsch-Bräuninger, M., Marzesco, A.-M., Bickle, M., Lohmann, A., Maliga, Z., Karbanová, J., Corbeil, D., Hyman, A. A. and Huttner, W. B. (2011). Proliferating versus differentiating stem and cancer cells exhibit distinct midbody-release behaviour. *Nat. Commun.* **2**, 443-446.
Finch, E. A., Turner, T. J. and Goldin, S. M. (1991). Calcium as a coagonist of inositol 1,3,4-trisphosphate-inducing calcium release. *Science* **252**, 443-446.
Fluck, R. A., Miller, A. L. and Jaffe, L. F. (1991). Slow calcium waves accompany cytokinesis in medaka fish eggs. *J. Cell Biol.* **115**, 1259-1265.
Fok, A. K., Aihara, M. S., Ishida, M. and Allen, R. D. (2008). Calmodulin localization and its effect on endocytic and phagocytic membrane trafficking in *Paramecium multimicronucleatum*. *J. Eukaryot. Microbiol.* **55**, 481-491.
Fransson, A., Ruusala, A. and Aspenström, P. (2003). Atypical Rho GTPases have roles in mitochondrial homeostasis and apoptosis. *J. Biol. Chem.* **278**, 6495-6502.
Galione, A., McDougall, A., Busa, W. B., Willmott, N., Gillot, I. and Whitaker, M. (1993). Redundant mechanisms of calcium-induced calcium release underlying calcium waves during fertilization of sea urchin eggs. *Science* **261**, 348-352.
Gilmour, D. T., Jessen, J. R. and Lin, S. (2002). Manipulating gene expression in the zebrafish. In *Zebrafish: Practical Approach Series*, Vol. 261 (ed. C. Nüsslein-Volhard and R. Dahm), pp. 121-143. Oxford: Oxford Press.
Gunter, T. E. and Pfeiffer, D. R. (1990). Mechanisms by which mitochondria transport calcium. *Am. J. Physiol.* **258**, C755-C786.
Harada, A., Furuta, B., Takeuchi, K.-I., Itakura, M., Takahashi, M. and Umeda, M. (2000). Nadrin, a novel neuron-specific GTPase-activating protein involved in regulated exocytosis. *J. Biol. Chem.* **275**, 36885-36891.
Hashimoto, Y., Maegawa, S., Nagai, T., Yamaha, E., Suzuki, H., Yasuda, K. and Inoue, K. (2004). Localized maternal factors are required for zebrafish germ cell formation. *Dev. Biol.* **268**, 152-161.
Heim, A. E., Hartung, O., Rothhämmel, S., Ferreira, E., Jenny, A. and Marlow, F. L. (2014). Oocyte polarity requires a Bucky ball-dependent feedback amplification loop. *Development* **141**, 842-854.
Henty-Ridilla, J. L., Rankova, A., Eskin, J. A., Kenny, K. and Goode, B. L. (2016). Accelerated actin filament polymerization from microtubule plus ends. *Science* **352**, 1004-1009.
Ichas, F., Jouaville, L. S. and Mazat, J.-P. (1997). Mitochondria are excitable organlles capable of generating and conveying electrical and calcium signals. *Cell* **89**, 1145-1153.
Ikebe, M. and Hartshorne, D. J. (1985). Phosphorylation of smooth muslce myosin at two distinct sites by myosin light chain kinase. *J. Biol. Chem.* **260**, 10027-10031.
Jaffe, L. F. (1993). Classes and mechanisms of calcium waves. *Cell Calcium* **14**, 736-745.
Jesuthasan, S. (1998). Furrow-associated microtubule arrays are required for the cohesion of zebrafish blastomeres following cytokinesis. *J. Cell Sci.* **111**, 3695-3703.
Jouaville, L. S., Ichas, F., Holmuhamedov, E. L., Camacho, P. and Lechleiter, J. D. (1995). Synchronization of calcium waves by mitochondrial substrates in Xenopus laevis oocytes. *Nature* **377**, 438-441.
Kane, D. A. and Kimmel, C. B. (1993). The zebrafish midblastula transition. *Development* **119**, 447-456.
Kimmel, C., Ballard, W. W., Kimmel, S. R., Ullmann, B. and Schilling, T. F. (1995). Stages of embryonic development of the zebrafish. *Dev. Dyn.* **203**, 253-310.
Knaut, H., Pelegri, F., Bohmann, K., Schwarz, H. and Nüsslein-Volhard, C. (2000). Zebrafish *vasa* RNA but not its protein is a component of the germ plasm and segregates asymmetrically before Germline Specification. *J. Cell Biol.* **149**, 875-888.
Kuo, T.-C., Chen, C.-T., Baron, D., Onder, T. T., Loewer, S., Almeida, S., Weismann, C. M., Xu, P., Houghton, J.-M., Gao, F.-B. et al. (2011). Midbody accumulation through evasion of autophagy contributes to cellular reprogramming and tumorigenicity. *Nat. Cell Biol.* **13**, 1214-1223.
Lawrence, E. J. and Mandato, C. A. (2013). Mitochondria localize to the cleavage furrow in mammalian cytokinesis. *PLoS ONE* **8**, e72886.
Lechleiter, J. D. and Clapham, D. E. (1992). Molecular mechanisms of intracellular calcium excitability in X. laevis oocytes. *Cell* **69**, 283-294.
Lee, K. W., Webb, S. E. and Miller, A. L. (2003). Ca^{2+} released via IP_3 receptors is required for furrow deepening during cytokinesis in zebrafish embryos. *Int. J. Dev. Biol.* **47**, 411-421.
Li, W. M., Webb, S. E., Chan, C. M. and Miller, A. L. (2008). Multiple roles of the furrow deepening Ca^{2+} transient during cytokinesis in zebrafish embryos. *Dev. Biol.* **316**, 228-248.
Lindeman, R. E. and Pelegri, F. (2012). Localized products of *futile cycle/lrmp* promote centrosome-nucleus attachment in the zebrafish zygote. *Curr. Biol.* **22**, 843-851.
Liu, X.-B. and Murray, K. D. (2012). Neuronal excitability and calcium/calmodulin/calmodulin-dependent protein kinase type II: location, location, location. *Epilepsia* **53** Suppl. 1, 45-52.
Lloyd-Burton, S. M., Yu, J. C. H., Irvine, R. F. and Schell, M. J. (2007). Regulation of inositol 1,4,5-trisphosphate 3-kinases by calcium and localization in cells. *J. Biol. Chem.* **282**, 9526-9535.
Macmillan, D. and Mccarron, J. G. (2010). The phospholipase C inhibitor U-73122 inhibits Ca^{2+} release from the intracellular sarcoplasmic reticulum Ca^{2+} store by inhibiting Ca^{2+} pumps in smooth muscle. *Br. J. Pharmacol.* **160**, 1295-1301.
Marlow, F. L. and Mullins, M. C. (2008). Bucky ball functions in Balbiani body assembly and animal-vegetal polarity in the oocyte and follicle cell layer in zebrafish. *Dev. Biol.* **321**, 40-50.
McVicker, D. P., Millette, M. M. and Dent, E. W. (2015). Signaling to the microtubule cytoskeleton: an unconventional role for CaMKII. *Dev. Neurobiol.* **75**, 423-434.
Mierzwa, B. and Gerlich, D. W. (2014). Cytokinetic abscission: molecular mechanisms and temporal control. *Dev. Cell* **31**, 525-538.
Mikl, M., Vendra, G. and Kiebler, M. A. (2011). Independent localization of *MAP2*, *CaMKII(alpha)* and *β-actin* RNAs in low copy numbers. *EMBO Rep.* **12**, 1077-1084.
Miranda-Rodríguez, J. R., Salas-Vidal, E., Lomelí, H., Zurita, M. and Schnabel, D. (2017). RhoA/ROCK pathway activity is essential for the correct localization of the germ plasm mRNAs in zebrafish embryos. *Dev. Biol.* **421**, 27-42.
Nair, S., Marlow, F., Abrams, E., Kapp, L., Mullins, M. C. and Pelegri, F. (2013). The chromosomal passenger protein Birc5b organizes microfilaments and germ plasm in the zebrafish embryo. *PLoS Genet.* **9**, e1003448.

Okabe, T., Nakamura, T., Nishimura, Y. N., Kohu, K., Ohwada, S., Morishita, Y. and Akiyama, T. (2003). RICS, a novel GTPase-activating protein for Cdc42 and Rac1, is involved in the β-catenin-N-cadherin and *N*-methyl-D-aspartate receptor signaling. *J. Biol. Chem.* **278**, 9920-9927.

Olsen, L. C., Aasland, R. and Fjose, A. (1997). A vasa-like gene in zebrafish identifies putative primordial germ cells. *Mech. Dev.* **66**, 95-105.

Otegui, M. S., Verbrugghe, K. J. and Skop, A. R. (2005). Midbodies and phragmoplasts: analogous structures involved in cytokinesis. *Trends Cell Biol.* **15**, 404-413.

Pelegri, F. and Schulte-Merker, S. (1999). A gynogenesis-based screen for maternal-effect genes in the zebrafish, *Danio rerio*. In *The Zebrafish: Genetics and Genomics*, Vol. 60 (ed. W. Detrich, L. I. Zon and M. Westerfield), pp. 1-20. San Diego: Academic Press.

Pelegri, F., Knaut, H., Maischein, H.-M., Schulte-Merker, S. and Nüsslein-Volhard, C. (1999). A mutation in the zebrafish maternal-effect gene *nebel* affects furrow formation and *vasa* RNA localization. *Curr. Biol.* **9**, 1431-1440.

Pelegri, F., Dekens, M. P. S., Schulte-Merker, S., Maischein, H.-M., Weiler, C. and Nüsslein-Volhard, C. (2004). Identification of recessive maternal-effect mutations in the zebrafish using a gynogenesis-based method. *Dev. Dyn.* **231**, 324-335.

Penny, C. J., Kilpatrick, B. S., Eden, E. R. and Patel, S. (2015). Coupling acidic organelles with the ER through Ca^{2+} microdomains at membrane contact sites. *Cell Calcium* **58**, 387-396.

Reinhard, E., Yokoe, H., Niebling, K. R., Allbritton, N. L., Kuhn, M. A. and Meyer, T. (1995). Localized calcium signals in early zebrafish development. *Dev. Biol.* **170**, 50-61.

Riemer, S., Bontems, F., Krishnakumar, P., Gömann, J. and Dosch, R. (2015). A functional Bucky ball-GFP transgene visualizes germ plasm in living zebrafish. *Gene Exp. Patterns* **18**, 44-52.

Scholey, J. M., Taylor, K. A. and Kendrick-Jones, J. (1980). Regulation of non-muscle myosin assembly by calmodulin-dependent light chain kinase. *Nature* **287**, 233-235.

Skop, A. R., Liu, H., Yates, J., III, Meyer, B. J. and Heald, R. (2004). Dissection of the mammalian midbody proteome reveals conserved cytokinesis mechanisms. *Science* **305**, 61-66.

Slusarski, D. C., Yang-Snyder, J., Busa, W. B. and Moon, R. T. (1997). Modulation of embryonic intracellular Ca^{2+} signaling by *Wnt-5A*. *Dev. Biol.* **182**, 114-120.

Steigemann, P. and Gerlich, D. W. (2009). Cytokinetic abscission: cellular dynamics at the midbody. *Trends Cell Biol.* **19**, 606-616.

Strome, S. and Lehmann, R. (2007). Germ versus soma decisions: lessons from flies and worms. *Science* **316**, 392-393.

Theusch, E. V., Brown, K. J. and Pelegri, F. (2006). Separate pathways of RNA recruitment lead to the compartmentalization of the zebrafish germ plasm. *Dev. Biol.* **292**, 129-141.

Tsunekawas, N., Noito, M., Sakai, Y., Nishida, T. and Noce, T. (2000). Isolation of chicken *vasa* homolog gene and tracing the origin of primordial germ cells. *Development* **127**, 2741-2750.

Urven, L. E., Yabe, T. and Pelegri, F. (2006). A role for non-muscle myosin II function in furrow maturation in the early zebrafish embryo. *J. Cell Sci.* **119**, 4342-4352.

Webb, S. E., Lee, K. W., Karplus, E. and Miller, A. L. (1997). Localized calcium transients accompany furrow positioning, propagation, and deepening during the early cleavage period of zebrafish embryos. *Dev. Biol.* **192**, 78-92.

Weidinger, G., Stebler, J., Slanchev, K., Dumstrei, K., Wise, C., Lovell-Badge, R., Thisse, C., Thisse, B. and Raz, E. (2003). *dead end*, a novel vertebrate germ plasm component, is required for zebrafish primordial germ cell migration and survival. *Curr. Biol.* **13**, 1429-1434.

Welling, M. and Geijsen, N. (2013). Uncovering the true identity of naïve pluripotent stem cells. *Trends Cell Biol.* **23**, 442-448.

Westfall, T. A., Hjertos, B. and Slusarski, D. C. (2003). Requirement for intracellular calcium modulation in zebrafish dorsal-ventral patterning. *Dev. Biol.* **259**, 380-391.

Whittington, P. M. and Dixon, K. E. (1975). Quantitative studies of germ plasm and germ cells during early embryogenesis of *Xenopus laevis*. *J. Embryol. Exp. Morph.* **33**, 57-74.

Wolff, A. M., Litske Petersen, J. G., Nilsson-Tillgren, T. and Din, N. (1999). The open reading frame of YAL048c affects the secretion of proteinase A in S. cerevisiae. *Yeast* **15**, 427-434.

Wühr, M., Tan, E. S., Parker, S. K., Detrich, H. W. I. and Mitchison, T. J. (2010). A model for cleavage plane determination in early amphibian and fish embryos. *Curr. Biol.* **20**, 2040-2045.

Wylie, C. (1999). Germ cells. *Cell* **96**, 165-174.

Yoon, C., Kawakami, K. and Hopkins, N. (1997). Zebrafish *vasa* homologue RNA is localized to the cleavage planes of 2- and 4-cell-stage embryos and is expressed in the primordial germ cells. *Development* **124**, 3157-3165.

Zhang, X.-F., Hyland, C., Van Goor, D. and Forscher, P. (2012). Calcineurin-dependent cofilin activation and increased retrograde actin flow drive 5-HT-dependent neurite outgrowth in *Aplysia* bag cell neurons. *Mol. Biol. Cell* **23**, 4833-4848.

Zhao, J.-W., Gao, Z.-L., Ji, Q.-Y., Wang, H., Zhang, H.-Y., Yang, Y.-D., Xing, F.-J., Meng, L.-J. and Wang, Y. (2012). Regulation of cofilin activity by CaMKII and Calcineurin. *Am. J. Med. Sci.* **344**, 462-472.